# PERFORMANCE OF STATIC DRILLED ROOT ENERGY PILES UNDER SEASONAL THERMAL LOADING: A STUDY OF MONOTONIC HEATING IN SUMMER

***Hong CHANG*[1], Yuan DU[1], Xing WU[1], Huicheng JIANG[1], Zhaoxuan WANG[1], Zhengheng GAN[1]***

[1] School of geomatics and prospecting engineering, Jilin Jianzhu University, Changchun 130118, China

[*] Corresponding author: changhong@jlju.edu.cn

*Energy piles are subjected to the combined effects of thermal and mechanical loads, requiring high load-bearing capacity and efficient heat transfer. This study introduces the concept of energy piles into static drill rooted piles (SDRP), forming a new structure known as static drilled rooted energy piles (SDREP). Model tests were conducted under monotonic heating cycles to evaluate their performance, primarily for summer cooling applications. The results show that the temperature distribution patterns of SDREP and ordinary energy piles (OEP) are generally similar. However, SDREP exhibits lower pile temperature fluctuations and a higher temperature field in the surrounding soil. Under heating cycles, the additional thermal stresses in SDREP gradually increase with the number of cycles, and the peak stress occurs closer to the pile tip. During 20 heating cycles, the soil pressure at the pile tip of SDREP was always lower than that of OEP. The pile head displacement also showed different behavior: the pile head displacement of SDREP increased upward, with a final displacement accumulation of 0.19% D. The pile head displacement of OEP showed a significant downward displacement, with a final displacement accumulation of 0.57% D. After 20 heating cycles, the ultimate bearing capacity of SDREP increased by 10%. These findings provide insight into the thermo-mechanical behavior of SDREP and provide theoretical support for its application in energy pile engineering.*

Key words*: static drilled rooted energy piles, thermo-mechanical behavior, monotonic heating cycles, model test*

## 1 Introduction

The energy pile uses the building pile foundation as a heat exchanger tube support, which has the advantages of cost savings, ease of construction, and a small footprint compared to the traditional ground source heat pump[1-3]. The new energy pile technology is gradually becoming an important technical means of exploiting shallow geothermal energy due to its dual function [4-7]. Moreover, this technology facilitates the advancement and development of energy storage, which is more in line with the goal of sustainable development[8-10].

During the operation of energy piles, temperature loads can affect the thermal-mechanical behavior of the piles[11]. Chang et al.[12] conducted model tests on energy piles subjected to different levels of mechanical loads and found that residual strains and stresses developed in the pile after thermal cycles. Zhang et al.[13] conducted field tests on energy piles subjected to separate and coupled thermo-

mechanical loads, and the results showed that coupled thermo-mechanical loads resulted in greater thermally induced stresses. In actual applications, energy piles not only bear vertical loads but also horizontal loads due to different functional requirements[14, 15]. Song et al.[16] conducted numerical simulations of inclined loads applied to energy piles, finding that different loading methods have varying effects on the thermo-mechanical behavior of energy piles. Loads applied in different directions significantly affect pile head displacement, with pile bending moments increasing during the heating phase and decreasing during the cooling phase. Additionally, the constraint forms at both ends of the pile also influence its thermo-mechanical behavior. Zhang et al.[17] conducted model tests to study the thermo-mechanical behavior of energy group piles with rigid pile caps. The results showed that rigid pile caps suppress the expansion and contraction of energy piles in response to temperature changes, thereby reducing their irreversible displacement. Ghezellou et al.[18] conducted model tests on energy piles with different end support conditions. The results showed that under the same mechanical load conditions, the maximum reduction in bearing capacity for semi-floating energy piles and end-bearing energy piles was 13.4% and 5.5%, respectively. Chang et al.[19] investigated the presence or absence of phase change materials (PCM) within steel pipe piles. The results showed that after the internal material of the energy pile was changed to PCM composite material, both the pile head displacement and maximum thermally induced stresses decreased. Kong et al.[20] conducted field tests on bell-shaped energy piles, and the results showed that, compared to straight energy piles, the displacement at the pile head of bell-shaped energy piles was lower than that of straight energy piles in three heating-cooling cycles. Jiang et al.[21] conducted a field test comparison between driven piles and bored piles, and the results showed that bored energy piles exhibit greater displacement. This indicates that different pile construction methods influence the thermos-mechanical behavior of energy piles.

In order to promote the use of energy piles, some scientists have conducted research on how to improve the heat exchange efficiency and mechanical properties of energy piles. Kong et al.[22] conducted numerical simulations of the thermal characteristics of energy piles with graphite as the variable, and the results showed that the addition of graphite increased the heat transfer efficiency of the energy piles by 6.5%. Lee et al.[23] utilized steel pipes, specifically steel pipe heat exchangers , to develop a novel energy pile. Chang et al.[24] conducted model experiments using steel pipe piles as heat exchanger tubes, and the results demonstrated that during the final heating cycle, the heat transfer efficiency of steel pipe energy piles was 32.6% higher than that of conventional energy piles. Yang et al. [25] demonstrated that phase change energy piles can improve heat transfer performance and reduce thermal deformation and additional thermal stresses at the tip of the pile using the established phase change energy pile model test system. Shahidiet al. [26] added lauric acid to concrete energy piles and constructed an indoor test apparatus to examine the thermo-mechanical behavior of phase change energy piles. The findings indicated that the phase change material mitigated temperature fluctuations and enhanced the thermal performance of the heat transfer system.

Previous studies have demonstrated the effectiveness of various technologies in improving the heat transfer capacity and thermo-mechanical performance of energy piles. However, both the use of phase change materials and changes to the structural materials of the pile body have certain limitations [24, 27, 28]. In contrast, the heat transfer performance and bearing capacity of static drilled rooted energy piles are superior to those of ordinary energy piles[29]. A contact thermal resistance exists between ordinary precast piles and the surrounding soil layer, which can be overcome by the use of static drilled rooted piles [30]. This phenomenon can be attributed to the filling of the gap between the

static drilled pile and the soil with a cement paste, which serves to facilitate the transfer of heat to the pile [31, 32]. Furthermore, in practical engineering applications in southeastern China, static drilled rooted nodular (SDRN) piles have demonstrated notable economic and environmental advantages. Data from a power plant project show that SDRN piles can reduce construction costs by approximately 10% compared to conventional bored piles while still meeting design requirements. In addition, soil displacement is only about 35.7% of the slurry emissions generated by traditional bored piling methods. These findings underscore the considerable economic and ecological benefits of promoting the static drilled rooted construction technique.[33]

At present, some progress has been made in the study of the thermo-mechanical properties of SDREP under hot and cold temperature cycling conditions, but fewer studies have been carried out on the relevant aspects of SDREP under monotonic thermal load. In particular, further investigation is required to ascertain the effect of the flared bottom portion of the pile tip on static drilled piles under continuous heating conditions. SDREP is a relatively straightforward construction, exhibits high bearing capacity, and shows considerable promise for geothermal utilization in the southeastern coastal region. Accordingly, this study considers the thermo-mechanical behavior of SDREP under monotonic heating conditions. This study investigated the temperature distribution of piles and soil, additional thermal stresses, and thermally mobilized shaft friction. This study provides a reference for the operational safety of SDREP, particularly in the context of summer conditions.

## 2 Model Tests

### 2.1 Model pile

The manufacturing process of the model piles is given in Figure. 1 The reinforcing framework used was 6 mm diameter main bars and wires. The SDREP system consists of a precast bamboo pile embedded within a cement-soil composite. The diameter of the composite pile is 84 mm, while the diameter of the precast bamboo pile is 44 mm. Each bamboo segment features a projection with a diameter of 48 mm, and a total of four such projections are distributed at intervals of 80 mm along the pile shaft. These protruding bamboo projections promote the formation of an integrated structure between the energy pile and the cement-soil matrix during installation, thereby enhancing the overall integrity of the composite pile system. The diameter of the OEP is 84mm, the length of both piles is 600mm, and the depth of the entry is 550mm. Prefabricated bamboo piles are manufactured by cutting PVC pipe into sections and then joining them together. The heat exchanger hose is constructed from PVC with an internal diameter of 8 mm. After initial setting on the second day, the model piles were demolded and subsequently cured under standard conditions for 28 days. The ordinary energy pile (OEP) utilizes single U-shaped heat exchanger tubes, which are bonded and integrated into individual units within the reinforced steel framework. SDREP employs double-spiral heat exchanger tubes that are fixed in a helical configuration around the outer surface of the bamboo piles before insertion into borehole filled with cement soil. The piles are then installed into pre-drilled, enlarged-bottom boreholes.

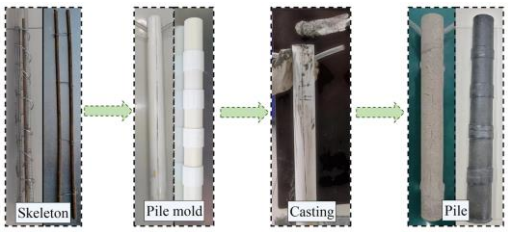


**Figure. 1 Model pile production process**

### 2.2 Model tank

The circular model tank is encased by acrylic panels and iron clamps, with a diameter and height of 600mm and 750mm, respectively. The exterior of the model tank was insulated with asbestos in order to prevent the external temperature from influencing the experimental setup. In order to prevent soil moisture loss, two layers of plastic film were applied to the interior of the model tank. The soil samples were dried in their natural state and then ground into fine powder. Water was subsequently added and thoroughly mixed with the soil to match the natural moisture content of the in-situ soil. To ensure uniform moisture distribution, the prepared soil was wrapped in plastic film and allowed to equilibrate for 2 hours. After confirming uniform moisture content, the soil was placed into the model water tank in layers. The soil was placed in the modeled trench in 10 layers, each layer measuring 70 mm in thickness. Upon completion of the filling process, it is necessary to activate the temperature circulation system. The temperature field of the pile soil was stabilized by circulating a heat transfer fluid at a temperature of 19.5°C. The soil parameters are shown in Table 1. The thermal conductivity of clay is measured by the YM-A type geotechnical thermal conductivity tester, and the specific heat capacity is measured by the BRR-III geotechnical specific heat capacity tester.

**Table 1. Properties of soil used in the test**

| Physical quantity | Value |
|---|---|
| Density, ρ [g/cm$^3$] | 1.90 |
| Moisture content, ω [%] | 29.4 |
| Thermal conductivity, [W/(m K)] | 1.21 |
| Specific heat capacity, [J/(kg K)] | 1430 |
| Specific gravity, Gs | 2.73 |
| Liquid limit, $W_L$ [%] | 41.9 |
| Plastic limit, $W_P$ [%] | 22.3 |
| Cohesion, c [kPa] | 33.13 |
| Angle of internal friction, φ [°] | 11.53 |

### 2.3 Test Instrument Systems

The instruments used in the experiment and their layout are shown in Figure. 2 The loading system consisted of calibrated weights and a loading plate. The displacement measurement system included 2 dial gauges positioned on opposite sides of the pile head, with the average of their readings taken as the pile head displacement. A total of 15 temperature sensors were installed along the pile shaft and in the surrounding soil to monitor both pile and soil temperatures. 5 strain gauges were affixed to the main reinforcement bars within the pile to measure the axial strain along the pile. A soil pressure cell was installed at the pile tip to record variations in tip resistance during the test. Data were recorded using a DH5921B dynamic data acquisition system and a YG-M temperature acquisition unit. Water was used as the heat exchange fluid, and a low-temperature thermostat provided the circulating thermal field.


**Figure. 2 Panoramic view of the model test**

The primary sources of inaccuracy in this model test are environmental and measurement-related. In order to reflect the reliability of the modeling device, the combined measurement error of the model test is expressed by the relative error. In order to calculate the relative error, Eq. (1) [4] must be employed. Table 2 provides a comprehensive overview of the test items included in the model test, the type of instrument utilized, the measurement range, and the associated accuracy.

$$\delta_{Rx_i} = \frac{\varphi_x K_i}{x_i} \tag{1}$$

Where $\delta_{Rxi}$ is the measurement parameters relative error, $\varphi_x$ denotes the accuracy of the measuring instrument, $K_i$ is the maximum range of the measuring instrument, $x_i$ is the minimum measured value of the measuring instrument.

**Table 2 Instrument parameters in the test system**

| Testing type | Instrument model | Measuring range | Accuracy |
|---|---|---|---|
| Collector of strain and pressure | DH5921 | 0-50000 με | 0.05%FS |
| Pile and soil temperatures | YG-M | -50-200 ℃ | ±0.1℃ |
| Measurement of temperature | TZWZP-1 | -50℃-200℃ | ±0.1℃ |
| Measurement of strain | BFH120-50AA-D-D300 | 0-20000 με | 0.05% FS |
| Pile head displacement | 32BFF25 | 0-25.4mm | 0.01mm |
| Circulating constant liquid | BILON-W-2001S | -5-95℃ | ±0.1℃ |

## 2.4 Experimental process

Figure. 3 shows the measuring points arranged. In order to monitor the strain within the pile, strain gauges were installed at 125mm, 225mm, 325mm, 425mm, and 525mm from the head of the pile. A soil pressure cell was placed at the exact center of the pile tip to measure the variation of soil pressure at the pile tip during the cyclic process. Five temperature sensors were placed in the vertical plane at 0.5D (42mm), 1.5D (126mm), and 2.5D (210mm) from the center axis of the pile at the same depth as the strain gauges to monitor the temperature change of the soil around the pile.

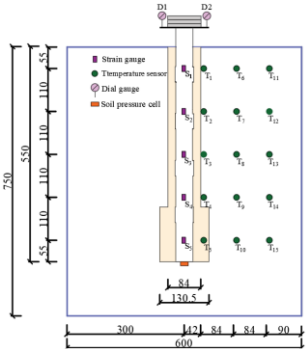


**Figure. 3 Measuring point layout**

The SDREP piling process is carried out in 4 steps: drilling, soil spreading, grouting, and piling. At the center of the model foundation was an 84 mm diameter and 550 mm high borehole, which was drilled using a soil extractor. The bottom of the borehole was enlarged to create an expanded base. The diameter of the enlarged section was 130.5 mm, which is 1.5 times the diameter of the borehole. The height of the expanded base was 144 mm, corresponding to 3 times the diameter of the bamboo projection [34]. Subsequently, a cement soil mixture composed of cement paste and clay slurry was injected into the structure. The parameters of the cement slurry are shown in Table 3. Then, a prefabricated bamboo pile equipped with heat exchange pipes and strain gauges was vertically inserted into the borehole and cured for 14 days to form a composite pile.

**Table 3. Parameters of the cement soil**

| Place | Water-cement ratio of cement paste | V (cement paste): V (slurry) | Cement Admixture (%) | Cement paste (με/°C) |
|---|---|---|---|---|
| Pile side | 1.0 | 0.3 | 11.54 | 6 |
| Pile tip | 0.6 | 1.0 | 45.81 | 6 |

### 2.5 Test Schedule

SDREP is mainly used in deep clay areas along the coast where summer working conditions prevail. Therefore, this study simulates the model pile to investigate the thermo-mechanical properties of SDREP after multiple cycles under monotonic heat production conditions. To guarantee the suitability of the test procedure, a preliminary trial was conducted to utilize the stability of the pile head displacements as a foundation for establishing the thermal load duration prior to the formalization of the test procedure. After a number of trials, it was finally decided that the conditions for a single cycle of heating for 4 hours and natural recovery for 8 hours were ideal. The scaling factor between the model and the prototype was determined based on the equal Fourier number principle, as proposed by Ding et al.[35] and Chang et al.[36]. The corresponding calculation Eq. (2) is as follows:

$$\frac{T_m}{T_p} = \frac{\left(r_m\right)^2}{\left(r_p\right)^2} \tag{2}$$

Where $T_m$ is the operating time of the model pile, h; $T_p$ is the operating time of the full-scale energy pile, h; $r_m$ is the radius of the model pile, mm; $r_p$ is the radius of the full-scale energy pile, mm.

Based on a model pile diameter of 44 mm and an operating time of 4 hours per cycle, the similarity ratio was determined to be 13.3. This implies that a full-scale energy pile with a diameter of 0.8 m and a length of 8.0 m would operate for approximately two months per cycle. Vertical static load tests were carried out on the modelled piles to determine the ultimate bearing capacity of a single pile prior to the start of the heating cycles. Take the working load as half of the ultimate bearing capacity of a single pile (Working load of 750N). The test program is displayed in Table 4.

**Table 4 Test basic information**

| Number | pile type | Pile length | Pile diameter | working load | Number of cycles |
|---|---|---|---|---|---|
| 1 | OEP | 600 mm | 84 mm | 600 N | 20 |
| 2 | SDREP | 600 mm | 44 mm | 750 N | 20 |

## 3 Results and discussion

### 3.1 Pile and soil temperatures

The variation rule of the pile temperature with time at different depths is basically the same, in Figure. 4 The amount of change in pile temperature was greatest at the beginning of the heating cycle compared to the beginning of the natural recovery phase. Upon completion of each natural recovery period, the pile temperature did not revert to its original state, and a build-up of heat occurred within the pile following the application of thermal cycling. The maximum temperature at each depth of the pile exhibited a gradual increase with the number of cycles under monotonic heating conditions. To illustrate, consider the relative depth $Z/L_1$=0.5 (at the T3 measurement point), the temperature increase was more

pronounced in the initial 10 cycles, The temperature at the peak point increased from 29.5°C to 32.6°C, with a cumulative increase of 3.1°C. The 20th cycle exhibited a maximum temperature of 33.3°C and a cumulative amount of 0.3°C cover 7 cycles. The temperature of the pile appears to stabilize after 17 cycles, with the maximum temperature of the 20th cycle being 33.4°C, an accumulation of only 0.1°C in 3 cycles. It is important to note that as the number of cycles increases, the temperature of the pile rises, resulting in the accumulation of heat. This, in turn, causes a gradual decrease in the temperature difference between the pile and the heat exchange fluid, which ultimately hinders the heat exchange process.

For each heat production cycle, the maximum temperature was identified at the T3 measurement point, with the pile tip temperature being less than the pile head temperature. The consideration is that the heat dissipation conditions are better at the ends of the pile than in the middle of the pile. The effect of air in the upper part of the pile must be taken into account. A portion of the heat transferred by the heat exchange fluid is dissipated during its transition from the upper to the lower portion of the system. On the other hand, the thermal conductivity of the pile tip cement soil is superior to that of the pile side cement soil. In summary, the temperature rises rapidly at the beginning and then slowly thereafter in a cycle. A comparison of the peak temperatures during the cycles shows that the peak temperatures during the first 20 cycles continue to rise. This will gradually weaken the temperature difference between the circulating fluid and the pile to a certain extent. It can be anticipated that the heat exchange performance may be weakened after 20 cycles.

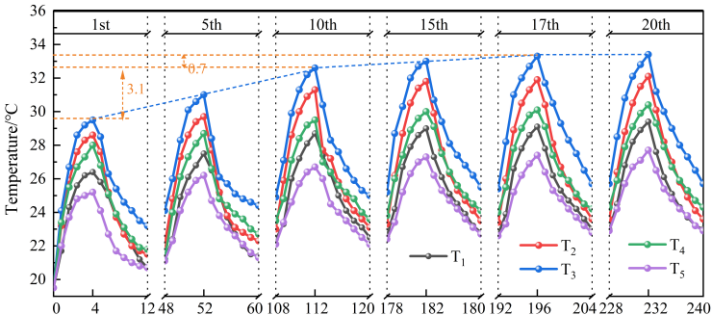


**Figure. 4 Variation of SDREP temperature with time**

The temporal variation of soil temperature around the pile at a depth of $Z/L_1$=0.5, in Figure. 5. The temperature of the soil in the vicinity of the pile and the temperature of the pile exhibit a similar trend, with both increasing and then decreasing. However, the time required to reach the peak point differs, in Figure. 5(a). Upon completion of the thermal cycle, the temperature of the pile begins to decline, while that of the soil continues to rise. It is postulated that the pile will possess a higher temperature than the soil at the conclusion of the thermal cycle. Furthermore, it is assumed that the heat will continue to spread to the distant soil, which reflects the process of heat dissipation from the pile. The soil exhibits a low heat transfer coefficient, with a correspondingly slower temperature rise the further one is from the pile center axis. The maximum temperature of the soil in the vicinity of the pile was 24.5°C at T8 and 20.5°C at T13 following 20 heating cycles, in Figure. 5(b).

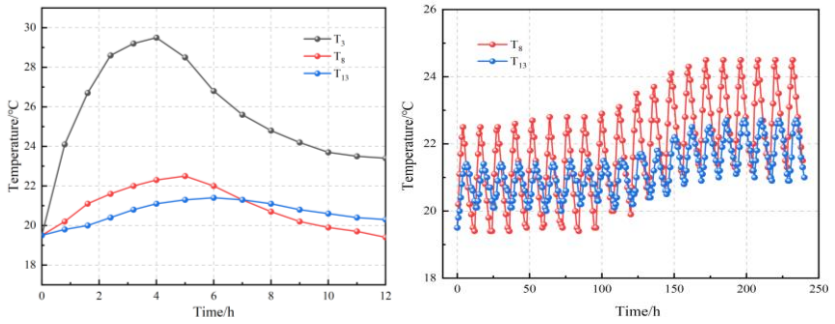


**Figure. 5 Variation of soil temperature over time at SDREP; (a) During the 1st cycle (b) During the 20th cycle**

At the conclusion of the initial temperature cycle, the distribution of OEP and SDREP temperature changes along the depth at 0.5D, 1.5D, and 2.5D from the center axis of the pile is illustrated in Figure. 6. At a distance of 0.5D from the pile axis, the maximum temperature change of OEP is 11.5°C, which represents a 15% increase in comparison to the SDREP. The maximum temperature change of the soil in the vicinity of the OEP pile at 1.5D and 2.5D from the axis of the pile was 4.8°C and 2°C, respectively, less than that of the SDREP (5.2°C and 2.3°C). It takes into account the presence of cement soil around the SDREP, which makes the heat transfer performance due to the OEP. The SDREP process transfers more heat to the surrounding cement soil. This results in lower pile temperatures and higher soil temperatures in the vicinity of the pile.

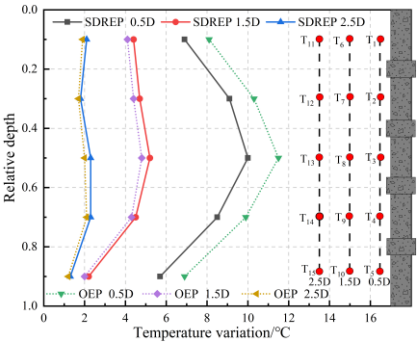


**Figure. 6 Temperature distribution along the depth at different radial distances (end of the 1st cycle)**

### 3.2 Additional thermal stresses of pile

Thermal expansion and contraction of the pile occur under thermal load, resulting in the generation of additional thermal stresses within the pile due to the constraint of the soil at the head of the pile and around the pile. This is calculated using the following formula:

$$\sigma_T = E(\varepsilon_{T-\text{free}} - \varepsilon_{T-\text{obs}}) \tag{3}$$

$$\varepsilon_{T-\text{free}} = \alpha_c \Delta T \tag{4}$$

Where: $E$ is the modulus of elasticity; $\varepsilon_{T\text{-}free}$ is the free strain; $\varepsilon_{T\text{-}obs}$ is the observed strain; $\alpha_c$ is the coefficient of thermal expansion; $\Delta T$ is the temperature difference between measurement points(℃). This defines the tensile stress generated in the pile as positive and the compressive stress as negative.

The pattern of variation of SDREP and OEP demonstrates a different trend with regard to additional thermal stresses at the moment of the end of the thermal cycle, in Figure.7. Both SDREP and OEP demonstrate a pattern of increasing and then decreasing additional thermal stresses along the depth direction. However, the locations of their peak points differ. It can be observed that additional thermal stresses for both arise gradually and cumulatively with the increase in the number of temperature cycles. The maximum additional thermal stresses after 20 heating cycles were -862 kPa and -780 kPa for SDREP and OEP, respectively. It is postulated that the modulus of elasticity and coefficient of linear expansion of SDREP are greater than those of OEP.

The maximum additional thermal stresses were observed to occur in the range of 0.4 to 0.6 relative depth for OEP and 0.6 to 0.8 relative depth for precast piles. The findings demonstrate that the SDREP tip demonstrated elevated thermal stresses at the conclusion of the testing period in comparison to the OEP. This phenomenon may be attributed to the greater confining influence exerted by the flared bottom section at the end of the SDREP piles. The cement soil at the tip of the pile demonstrated enhanced confining characteristics when subjected to thermal loading. This outcome aligns with the findings of

analogous studies on flared-bottom piles [37]. Therefore, after 20 heating cycles, the additional thermal stress is likely to increase due to the continuous accumulation of temperature. In practical engineering applications, it is essential to monitor the peak thermal stress to ensure that it remains within a reasonable and safe range.

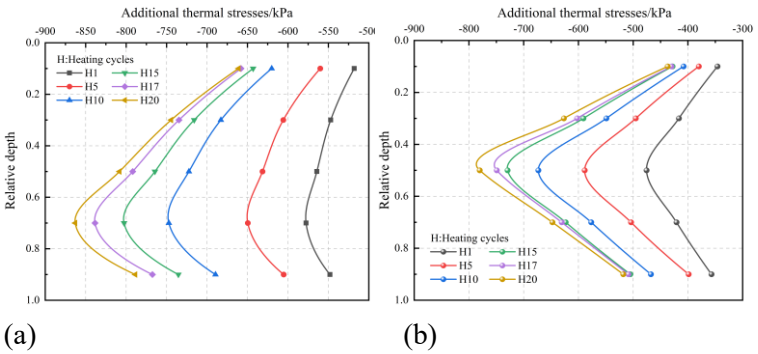


(a) (b)

**Figure. 7 Distribution of additional thermal stresses at the end of heating; (a) SDREP (b) OEP**

Figure 8 shows the additional thermal stresses and temperature change curves for SDREP and OEP. The measured relative depths are 0.1, 0.3, 0.5, 0.7, and 0.9. The fitting coefficients for $\sigma_T$ and $\Delta T$ corresponding to SDREP are -110, -88, -105, -141, and -164, respectively. The fitting coefficients for $\sigma_T$ and $\Delta T$ corresponding to OEP are -57, -60, -83, -86, and -81, respectively. The fitting coefficients represent the additional thermal stress caused by each unit of temperature increase. Overall, both SDREP and OEP exhibit an increase in the magnitude of additional thermal stress as the temperature change increases. Notably, under the same temperature change conditions, the additional thermal stress at each measurement point for SDREP is greater than that at the corresponding measurement points for OEP. This is because the outer layer of SDREP is enclosed by a layer of cement soil, resulting in greater constraint on the overall pile body compared to the constraint provided by the surrounding soil for OEP. The location of the maximum additional thermal stresses growth rate in SDREP is near the pile tip ($T_5$). While the maximum location of additional thermal stresses growth rate in OEP is near the center ($T_3$).

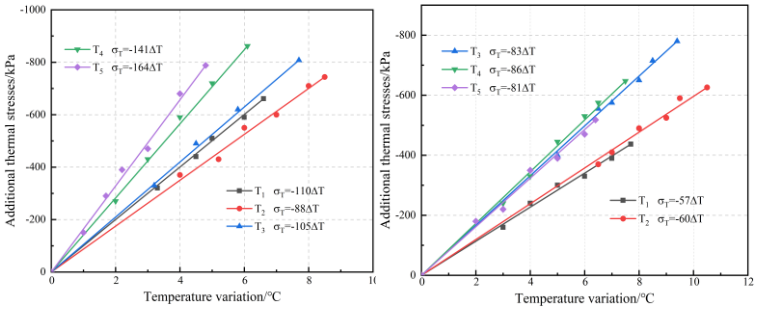


(a) (b)

**Figure.8 Relationship between additional thermal stresses and pile temperature variation; (a) SDREP (b) OEP**

### 3.3 Thermally mobilized shaft friction

The main difference between SDREP and OEP is the presence of two friction surfaces in SDREP. These two friction surfaces are the precast pile and cement soil friction surface and the cement soil and soil friction surface. Therefore, the load transfer mechanism of SDREP is different from that of OEP. The microelement force analysis of the precast pile and cement soil is shown in Figure. 9.

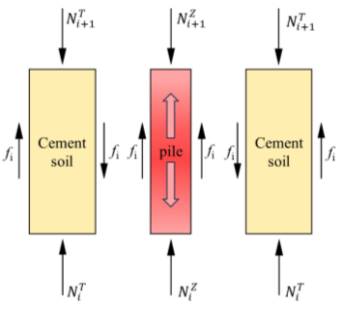


**Figure. 9 Microelement force analysis of SDREP**

In accordance with the principle of microporous force equilibrium, the equilibrium equations for the precast pile, cement soil, and soil surrounding the pile can be expressed as follows:

$$N_{i+1}^{Z} - N_{i}^{Z} = \pi d \Delta l f_i \tag{5}$$

$$N_{i+1}^{T} + \pi d \Delta l f_i = \pi D \Delta l f_j + N_{i}^{T} \tag{6}$$

Where: d is the diameter of precast pile (mm). $D$ is the diameter of static drilled pile (mm); $\Delta l$ is the length of calculation unit (mm). $N_{i+1}^{Z}$, $N_{i}^{Z}$ are the additional axial forces (N) in section $i$+1 and section i of the precast pile. $N_{i+1}^{T}$,$N_{i}^{T}$ are the additional axial forces (N) in section $i$+1 and section $i$ of the cement soil, respectively. $f_i$ is the precast pile and cement soil thermally mobilized shaft friction (kPa). $f_j$ is the cement soil and the soil around the pile thermally mobilized shaft friction.

During the temperature cycle, the pile was subjected to thermal expansion and relative displacement of the pile and soil occurred. This was constrained by the working load at the head of the pile and the expanded bottom at the tip of the pile, which limited the free displacement of the pile. This resulted in thermally mobilized shaft friction of the pile. In accordance with the provisions set forth in Eq. (7), the thermally mobilized shaft friction of SDREP and cement soil can be calculated in order to derive the distribution of thermally mobilized shaft friction along the pile. Figure. 10 illustrates the distribution of thermally mobilized shaft friction along the depth for SDREP and OEP at the conclusion of the heating.

$$f_{s,(z_{i+1}-z_i)} = \frac{(\sigma_{T,z_{i+1}} - \sigma_{T,z_i})D}{4(z_{i+1} - z_i)} \tag{7}$$

Where: $z_i$ is the burial depth of each strain gauge of the pile; $i$ =1,2,3,4 is the number of each strain gauge from top to bottom of the pile; $\sigma_{T,zi}$; is the thermo-mechanical stresses at depth $z_i$; $D$ is the diameter of the model pile(mm). In this test, thermo-mechanical frictional resistance is defined as positive in the upward direction and negative in the downward direction.

The SDREP expands from the neutral plane to both ends, creating negative lateral frictional resistance at the head of the pile and positive lateral frictional resistance at the bottom. Consistent with the pattern summarized by Webb et al. [38] and Amatya et al. [39], the thermally mobilized shaft friction pattern was demonstrated in this study. The DREP neutral point is in the range of 0.6 to 0.8 relative depth, while the OEP neutral point is in the range of 0.4 to 0.6 relative depth. The maximum thermally mobilized shaft friction at the top of the SDREP (17.5 kPa) is greater than the thermally mobilized shaft friction at the tip of the pile (15.6 kPa). The maximum thermally mobilized shaft friction at the top of the OEP is 39.8 kPa, and the thermally mobilized shaft friction at the tip of the pile (27 kPa) is greater than that of the SDREP. The strong confinement at the tip of the pile is taken into account, resulting in small relative displacements. The influence of the degree of constraint on the position of the neutral plane has been demonstrated in previous studies with similar methodologies [37, 40]. For both SDREP and OEP, the absolute values of side friction resistance at each measurement point exhibit a

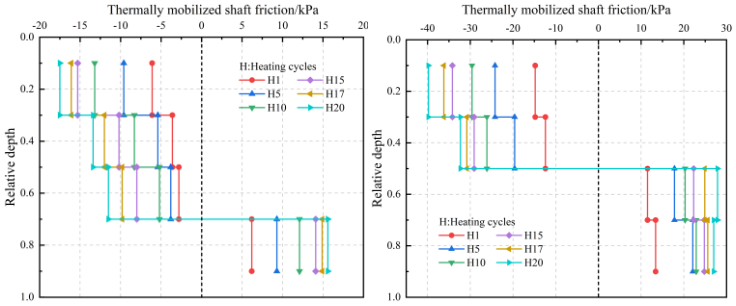


**Figure. 10 Distribution of thermally mobilized shaft friction along depth; (a) SDREP (b) OEP**

positive correlation with the number of heating cycles. This is attributed to thermal consolidation of the surrounding soil after 20 monotonic heating cycles, which enhances the lateral confinement on the pile.

As illustrated in Figure. 11, a clear correlation is observed between thermally mobilized shaft friction and temperature variations during both the SDREP and OEP heating processes. In the figure, μ represents the coefficient quantifying the increase in thermally mobilized shaft friction with temperature variation. In summary, thermally mobilized shaft friction demonstrated a direct and positive correlation with increasing temperature. During the heating phase, the upper sections of the SDREP and OEP piles exhibited upward displacement relative to the surrounding soil, while the lower section moved downward. This behavior is primarily attributed to thermal expansion of the pile. As a result, both the axial friction and the coefficient μ in the upper part of the pile are negative, whereas in the lower part they are positive. For SDREP, mobilized shaft friction increased by 2.35 kPa, 1.67 kPa, 1.81 kPa, and 3.00 kPa with depth for each 1°C temperature rise. Similarly, for OEP, the increases were 4.34 kPa, 3.19 kPa, 3.37 kPa, and 4.04 kPa. The μ values for SDREP and OEP remained positive at relative depths below 0.7 and 0.5, respectively. This behavior can be attributed to the bottom expansion structure of the SDREP, which effectively restrains movement in the lower part of the pile, thereby shifting the neutral point downward.

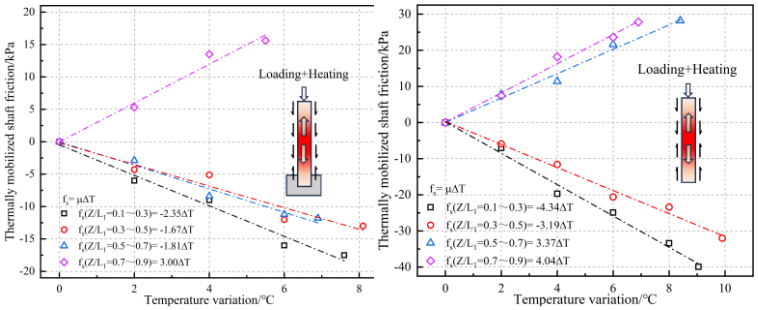


**Figure. 11 Linear relationship between thermally mobilized shaft friction and temperature variation;(a) SDREP (b) OEP**

### 3.4 Soil pressure at pile tip

As illustrated in Figure. 12, the variation in soil pressure at the pile tip for both OEP and SDREP under 20 heating cycles is presented. The soil pressure at the pile tip of the OEP increases progressively with the number of cycles, whereas the SDREP shows irregular fluctuations throughout the cycles. The soil pressure at the pile tip of the OEP was consistently greater than that of the SDREP during both the working and recovery stages. This difference can be attributed to two main factors. First, although both piles experienced significant axial expansion during the working stage, the axial deformation of the SDREP was less pronounced due to the stronger confinement provided by the surrounding hydraulic soil and the enlarged base at the pile tip. Second, due to the influence of lateral restraint, part of the load in the SDREP was redistributed from the pile tip to the pile shaft during load transfer. Furthermore, the pile tip of the OEP lacks a flared geometry, resulting in a smaller contact area and higher stress concentration compared to the SDREP. Thus, the combined effects of these factors cause the OEP's pile-tip soil pressure to remain higher than that of the SDREP. Meanwhile, the fluctuations in soil pressure at the SDREP pile tip are primarily attributed to the combined influence of lateral soil-pile interaction and the flared base structure. This configuration alters the stress transfer path, leading to uneven stress distribution within the surrounding soil and

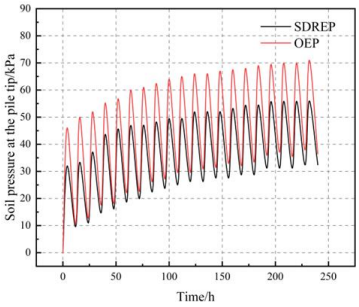


**Figure. 12. Distribution of soil pressure at pile tip under 20 cycles**

localized abrupt changes in soil pressure. In 20 cycles, the maximum values of soil pressure at pile tip for both SDREP and OEP appeared at the end moment of the 20th cycle, which were 56kPa and 71kPa, respectively. Therefore, SDREP has higher safety compared to OEP, and the introduction of SDREP can be considered to mitigate the damage to the soil at pile tip in soft soil areas.

The relationship between soil pressure at the pile tip and pile head displacement for both OEP and SDREP is illustrated in Figure. 13. In this study, upward displacement (heave) of the pile head is defined as positive, while settlement is defined as negative. The results indicate a positive correlation between pile tip soil pressure and pile head displacement for both pile types, under the combined influence of mechanical and thermal loading. The increase in soil pressure at the pile tip of the OEP primarily results from soil crowding induced by pile settlement. In contrast, the SDREP is constrained by the strong interaction between the hydraulic soil and the surrounding soil mass, which enables it to generate a significant pullout resistance during pile uplift. This behavior is reflected in the concurrent increase in soil pressure and pile head displacement during bulging. The OEP required 15 cycles to stabilize the soil pressure-displacement response, whereas the SDREP achieved stability after only 5 cycles. This difference is primarily attributed to the distinct constraint mechanisms at the pile side and pile tip of the two systems. The OEP relies on frictional contact at the pile-soil interface, which undergoes considerable plastic deformation during the initial cycles, thereby requiring more cycles to develop a stable stress field. In contrast, the SDREP features a higher-strength anchorage connection at the interface, allowing it to reach a stable response within fewer cycles. SDREP has better pile-soil co-deformation ability than OEP piles, and can quickly reach a stable state (displacement and soil pressure are no longer carried out significantly). In summary, the superior safety of SDREP highlights the advantages of its application in the long-term service of energy piles.

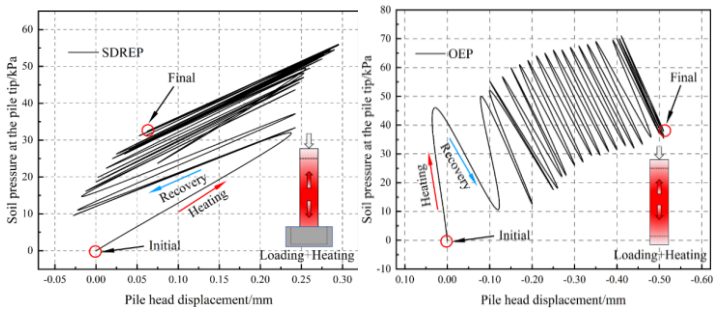


(a) (b)

**Figure 13 Pile tip Soil pressure with pile head displacement; (a)SDREP (b)OEP**

### 3.5 Pile head displacement

The vertical displacement versus time curves for the tops of the SDREP and OEP, in Figure.14. For each heating cycle, the pile head displacement shows an increase, and the pile head displacement returns to its initial position during the natural recovery phase. The OEP pile head displacement gradually accumulates downwards as the number of cycles increases. Maximum displacement occurred at the end of cycle 17 at -0.29mm (0.34% D); it has remained stable since then. The cumulative displacements at the head of the pile were -0.48 mm (0.57% D) at the end of the 20th natural recovery phase. SDREP displacement occurs at the same time as OEP but generally trends upwards. Maximum displacement was 0.16mm (0.19% D) and cumulative displacement was 0.03 mm (0.04% D). This consideration of the presence of cement-treated soil layers around the SDREP increases the constraining effect on the SDREP. Additionally, the presence of the pile tip flared base allows it to support the upper working load and restrict the displacement of the pile head. This is consistent with the patterns of lateral friction resistance. Therefore, during a monotonic heating cycle, the SDREP expands toward both ends

when heated, with the constraint at the pile tip exceeding the constraint provided by the upper load. Ultimately, after 20 heating cycles, this manifests as upward displacement of the pile head.

The OEP lacked a pile tip flare bottom, and the heating cycles caused the pile to expand radially. The soil surrounding the pile was subjected to shear forces over the course of multiple cycles. In addition, the direction of displacement of the pile is consistent with the direction of the vertical loads, causing the pile head to ultimately displace downward. Both SDREP and OEP piles exhibit a working load limitation at the pile head, which gradually stabilizes after the seven heating cycles. Combined with Figure. 4. it can be seen that the change characteristics of the pile head displacement basically coincide with the trend of the pile temperature change. The SDREP performed better than the OEP in terms of the displacement of the pile head after 20 cycles of heat production. This indicates that SDREP is more resistant to displacements at the head of the pile. Although the amount of change in pile head displacement is relatively small, it is still necessary to be aware of the dangers of superstructure displacement in real projects.

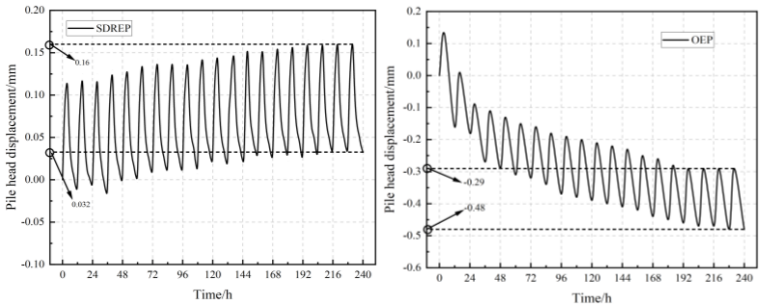


(a) (b)

**Figure. 14 Pile head position variation with the number of cycles; (a) SDREP (b) OEP**

### 3.6 Pile ultimate bearing capacity

To evaluate the effect of thermal cycles on the ultimate bearing capacity of energy piles, static load tests were conducted on both SDREP and OEP before and after 20 heating cycles. The corresponding load-displacement curves are presented in Figure. 15. For SDREP, the ultimate load increased from 1.50 kN (pre-cycle) to 1.65 kN after 20 cycles, representing a 10% improvement. This enhancement can be attributed to two main factors. On the one hand, the repeated heating cycles led to thermal consolidation of the surrounding soil, which increased interparticle friction [41]. On the other hand, the SDREP's larger specific surface area enhanced the effective contact interface between the pile and the soil. Supporting geotechnical tests confirmed that the internal friction angle of the soil increased after thermal cycles, while cohesion slightly decreased, which is consistent with the findings of Yazdani et al.[42] These changes suggest that repeated thermal cycling densifies the soil structure at the pile-soil interface, thereby improving load transfer and bearing capacity.

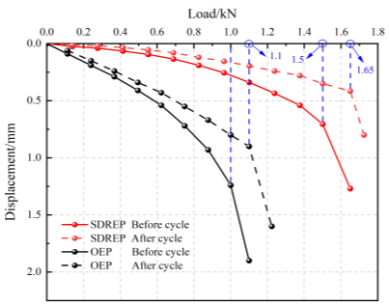


**Figure. 15 Load-displacement curves before and after heating cycles**

In contrast, the OEP showed a significant reduction in the ultimate bearing capacity after 20 heating cycles, reaching only 1.10 kN-approximately 33% lower than that of SDREP under identical conditions. This inferior performance is likely due to insufficient load transfer at the pile tip and weakened pile-soil interaction. The superior performance of SDREP highlights the mechanical advantages of its enlarged pile tip and improved interaction with thermally consolidated soil. These

results underscore the potential of SDREP for applications that demand both structural support and efficient heat exchange under repeated thermal loading conditions.

## 4 Conclusions and prospects

### 4.1 Conclusions

This model experiment studied SDREP under monotonic heating conditions. In order to draw practical conclusions, further comparisons were made with OEP. The main conclusions are as follows:

- After 20 heating cycles, the highest temperatures within both the pile and the soil were observed at a relative depth of 0.4 to 0.6. The soil temperature is significantly influenced by SDREP at varying radial distances.
- Under monotonic heating conditions, the distribution of additional thermal stress gradually increases with the number of heating cycles. The maximum additional thermal stress occurs at different relative depths for SDREP and OEP: 0.6-0.8 for SDREP and 0.4-0.6 for OEP.
- The distribution patterns of additional shaft friction for SDREP and OEP are similar, but the location of the neutral plane differs. The neutral plane of the SDREP tends to be located closer to the lower part of the pile. As the number of heating cycles increases, the growth rate of the thermally induced shaft resistance in the SDREP gradually decreases.
- As the number of cycles increases, the soil pressure at the pile tips of OEP and SDREP gradually increases. After 20 heating cycles, the soil pressures of OEP and SDREP are 56 kPa and 71 kPa, respectively. This indicates that SDREP has better safety performance than OEP, which is beneficial to safety in actual engineering.
- The displacement patterns of SDREP and OEP pile heads differ. While SDREP pile head displacement occurs during downward movement, it is hindered by the flared pile tip. Ultimately, after 20 heating cycles, the cumulative displacement slightly increases to 0.19% D. OEP pile head displacement accumulates significantly downward with increasing cycle counts, reaching a maximum displacement of 0.57% D after 20 heating cycles.
- After 20 heating cycles, the ultimate bearing capacity of both the SDREP and the OEP was increased to varying degrees, up to 10%. The bearing capacity of the SDREP is 50% higher than the OEP, demonstrating the good load bearing capacity of the SDREP.

### 4.2 Prospects

In this study, the modeled static drilled rooted method was used in conjunction with energy pile technology to investigate the performance of static drilled rooted energy piles using seasonal thermal loading as the study condition. The model provides a prior investigation for exploring the improvement of heat transfer capacity and good thermal-mechanical behavior of energy piles. To promote the use of this new energy pile in monotonic heating conditions is the main mode of operation. And to provide considerable reference for the design and construction of real projects.

The results showed that the soil temperature around the SDREP was higher, indicating its favorable heat transfer performance. However, the heat transfer mechanism was not examined in detail in this study. In addition, due to the presence of surrounding cement soil layers, the boundary conditions of the SDREP differ from those of conventional energy piles. The load transfer mechanism under thermal loading remains unclear, and the simplified boundary conditions adopted in this experimental

setup allowed only for a preliminary analysis. In future work, we plan to further investigate the influence of the surrounding cement soil on the heat transfer behavior of energy piles and to develop a theoretical model to better describe the mechanical constraints imposed by the cement-soil interface. Moreover, full-scale field tests and long-term monitoring under real operating conditions will be conducted to validate the model and gain a more comprehensive understanding of SDREP performance.

**Acknowledgment**

This study was financially supported by the Science and Technology Department of Jilin Province(No. 20230203045SF).

**Nomenclature**

| | | | |
|---|---|---|---|
| *Acronyms* | | $\sigma_T$ | —Additional thermal stress of the pile |
| SDRP | —Static drill rooted pile | $\varepsilon_{T\text{-free}}$ | —Free strain of the pile |
| SDREP | —Static drilled rooted energy pile | $\varepsilon_{T\text{-obs}}$ | —Observed strain of the pile |
| OEP | —Ordinary energy pile | $f_{s,(z_i-z_{i+1})}$ | —Average side friction on the pile side |
| L | —Length of the model pile | $z_i$ | —The depth of strain gauge i |
| $L_1$ | —Depth of pile into the ground | *Greek symbols* | |
| D | —The pile diameter | c | —Force cohesion |
| E | —Modulus of elasticity | φ | —Angle of internal friction |
| ΔT | —Temperature value | $\alpha_c$ | —Coefficient of thermal expansion |

**References**

[1] Ai, Z.Y.,W.Y. Feng, The mechanical response of energy pile groups in layered cross-anisotropic soils under vertical loadings, *Energy*, *292*. (2024), p. 130531.

[2] Luu, G.T., *et al.*, Enhancing long-term viability of energy pile with heat sink systems in tropical monsoon climates: Implementation strategies and performance analysis, *Energy and Buildings*, *328*. (2025), p. 115119.

[3] Cao, X., *et al.*, Feasibility assessment of implementing energy pile-based snowmelt system on a practical bridge deck in diverse climate conditions across China, *Energy*, *290*. (2024), p. 130317.

[4] Chang, H., *et al.*, Experimental study of phase change energy pile based on Gum Arabic and Polyethylene Glycol 600 under multiple Thermal-Cold cycles, *Construction and Building Materials*, *438*. (2024), p. 137109.

[5] Fadejev, J., *et al.*, A review on energy piles design, sizing and modelling, *Energy*, *122*. (2017), pp. 390-407.

[6] Kong, G., *et al.*, Seasonal performance of an energy pile heat pump system and prediction of building thermal load, *Applied Thermal Engineering*, *241*. (2024), p. 122359.

[7] Song, H., *et al.*, Thermomechanical analysis of dissimilar energy pile groups using a load transfer method, *Renewable Energy*, *254*. (2025), p. 123708.

[8] Han, C.,X. Yu, An innovative energy pile technology to expand the viability of geothermal bridge deck snow melting for different United States regions: Computational assisted feasibility analyses, *Renewable Energy*, *123*. (2018), pp. 417-427.

[9] Wang, Z., *et al.*, Influence of silicon carbide incorporation on the macroscale and microscale heat transfer characteristics of energy piles, *Renewable Energy*, *237*. (2024), p. 121717.

[10] Zhang, R., *et al.*, Experimental study on energy pile thermal-structure response during high temperature heat storage, *Journal of Energy Storage*, *120*. (2025), p. 116458.

[11] He, F., *et al.*, Effects of thermal loading conditions on the thermo-mechanical response of energy pile at different depths, *Geothermics*, *131*. (2025), p. 103392.

[12] Chang, H., *et al.*, Thermo-mechanical response of energy piles under monotonic cooling cycles and various mechanical loading levels, *Journal of Energy Storage*, *113*. (2025), p. 115672.

[13] Zhang, G., *et al.*, Full-scale tests of a long energy pile subjected to separated and coupled thermo-

mechanical loads, *Proceedings of the Institution of Civil Engineers - Geotechnical Engineering*, *177*. (2024), 5, pp. 564-577.
[14] Dupray, F., *et al.*, Heat-exchanger piles for the de-icing of bridges, *Acta Geotechnica*, *9*. (2014), pp. 413-423.
[15] Zhao, H., *et al.*, An approach for analysis of a single energy pile subjected to a horizontal load in sand, *Case Studies in Thermal Engineering*, *56*. (2024), p. 104289.
[16] Song, H., *et al.*, Long-term thermomechanical behavior of energy piles under inclined load, *Journal of Energy Storage*, *99*. (2024), p. 113258.
[17] Zhang, D., *et al.*, Influence of a rigid cap on thermo-mechanical behavior of nonsymmetrical thermally loaded energy pile group in clay, *Canadian Geotechnical Journal*, *60*. (2022), 5, pp. 654-668.
[18] Ghezellou, A., *et al.*, Thermomechanical response of energy piles in dry sand under monotonic cooling with varying end-support conditions, *Journal of Energy Storage*, *82*. (2024), p. 110469.
[19] Chang, H., *et al.*, Experimental study on the thermo-mechanical behavior of steel pipe energy pile groups with and without phase change material, *Geothermics*, *129*. (2025), p. 103304.
[20] Kong, G., *et al.*, Behaviours of a belled energy pile under heating-cooling cycles, *Journal of Building Engineering*, *72*. (2023), p. 106652.
[21] Jiang, G., *et al.*, Thermo-mechanical behavior of driven energy piles from full-scale load tests, *Energy and Buildings*, *233*. (2021), p. 110668.
[22] Kong, L.-p., *et al.*, A study on heat transfer characteristics and pile group influence of enhanced heat transfer energy piles, *Journal of Building Engineering*, *24*. (2019), p. 100768.
[23] Lee, S., *et al.*, Dual performance of novel steel pipe heat exchangers equipped in cast-in-place energy pile, *Energy and Buildings*, *234*. (2021), p. 110725.
[24] Chang, H., *et al.*, Thermo-mechanical behavior of PCM-enhanced steel pipe energy piles, *Applied Thermal Engineering*, *276*. (2025), p. 126917.
[25] Yang, W., *et al.*, Numerical evaluations on the effects of thermal properties on the thermo-mechanical behaviour of a phase change concrete energy pile, *Energy and Built Environment*, *4*. (2023), 1, pp. 1-12.
[26] Shahidi, S., *et al.*, Experimental investigation on the efficiency of the phase change materials for enhancing the thermal performance of energy piles in sandy soils, *ENERGY AND BUILDINGS*, *298*. (2023).
[27] Xia, C., *et al.*, Investigation of heat transfer characteristics in steel fiber-reinforced energy piles utilizing steel tubes for PCM encapsulation, *Energy*, *326*. (2025), p. 136273.
[28] Lee, S., *et al.*, Data-driven prediction of long-term thermal performance for steel pipe heat exchanger (SPHX) energy piles, *Geothermics*, *129*. (2025), p. 103292.
[29] Chang, H., *et al.*, Thermo-mechanical response of static drilled rooted energy piles under monotonic cooling cycle, *Construction and Building Materials*, *456*. (2024), p. 139276.
[30] Zhang, Q., *et al.*, Thermal performance and applied evaluation of the pre-bored grouting planted nodular pile in warm frozen soil, *Applied Thermal Engineering*, *248*. (2024), p. 123178.
[31] Zhou, J.-j., *et al.*, Bearing capacity and load transfer mechanism of a static drill rooted nodular pile in soft soil areas, *Journal of Zhejiang University SCIENCE A*, *14*. (2013), 10, pp. 705-719.
[32] Yu, J.-l., *et al.*, The frictional capacity of smooth concrete pipe pile–cemented soil interface for pre-bored grouted planted pile, *Acta Geotechnica*, *18*. (2023), 8, pp. 4207-4218.
[33] Zhou, J.-j., *et al.*, A field study on the behavior of static drill rooted nodular piles with caps under compression, *Journal of Zhejiang University-SCIENCE A*, *16*. (2015), 12, pp. 951-963.
[34] Zhou, J., *et al.*, Model tests comparing the behavior of pre-bored grouted planted piles and a wished-in-place concrete pile in dense sand, *Soils and Foundations*, *59*. (2019), 1, pp. 84-96.
[35] Ding, X., *et al.*, Thermo–mechanical behavior of energy pile group in dry sand subjected to a horizontal load, *Renewable Energy*, *233*. (2024), p. 121170.
[36] Chang, H., *et al.*, Thermo-mechanical behavior of steel pipe energy piles under thermal imbalance cycles, *Construction and Building Materials*, *447*. (2024), p. 138026.
[37] Kong, G., *et al.*, Behaviours of a belled energy pile under heating-cooling cycles, *Journal of Building Engineering*, *72*. (2023).
[38] Bourne-Webb, P.J., *et al.*, A framework for understanding energy pile behaviour, *PROCEEDINGS OF THE INSTITUTION OF CIVIL ENGINEERS-GEOTECHNICAL ENGINEERING*, *166*. (2013), 2, pp. 170-177.
[39] Amatya, B.L., *et al.*, Thermo-mechanical behaviour of energy piles, *Géotechnique*, *62*. (2012), 6, pp. 503-519.
[40] Zhang, D., *et al.*, Influence of a rigid cap on thermo-mechanical behavior of nonsymmetrical thermally loaded energy pile group in clay, *Canadian Geotechnical Journal*, *60*. (2023), 5, pp. 654-668.

[41] Abu-Farsakh, M.Y.,A. Idries, Enhancement of clay-concrete interface strength through applying cycles of heating and cooling, *Geothermics*, *113*. (2023), p. 102772.
[42] Yazdani, S., *et al.*, Influence of temperature on soil–pile interface shear strength, *Geomechanics for Energy and the Environment*, *18*. (2019), pp. 69-78.

Submitted: 16.05.2025.
Revised: 23.07.2025.
Accepted: 24.07.2025.